JTTEE5 20:549–559
DOI: 10.1007/s11666-010-9572-2
1059-9630/$19.00 © ASM International

Influence of Plasma Intensity on Wear and Erosion Resistance of Conventional and Nanometric WC-Co Coatings Deposited by APS

V. Bonache, M.D. Salvador, J.C. García, E. Sánchez, and E. Bannier

(Submitted May 31, 2010; in revised form September 13, 2010)

The effects of plasma intensity and powder particle size on wear and erosion resistance have been evaluated for WC-12 wt.%Co coatings deposited by Air Plasma Spraying. Coatings were deposited from micrometric and nanostructured powders. SEM and XRD characterization showed the presence of WC, W_2C, W, and an amorphous Co-rich matrix. The performance of the different coatings was compared in sliding wear tests (ball-on-disk), under dry friction conditions. Wear debris and tracks were analyzed by SEM. The debris generated during the test was found to have a great influence on the sliding properties. Wear follows a "three-body abrasive mechanism" and is dominated by coating spallation because of subsurface cracking. In order to evaluate erosion behavior, solid particle erosion tests were conducted. Eroded coatings were analyzed by SEM, and erosion mainly occurs by a "cracking and chipping mechanism." The study shows that wear and erosion behavior is strongly affected by plasma arc intensity.

Keywords cermets, erosion testing, nanostructure, plasma spray coatings, wear testing

1. Introduction

WC-Co coatings deposited by thermal spraying have been widely used in wear situations because they combine several advantages such as resistance to abrasion, erosion, and high temperature (Ref 1, 2). The thermal spray process involves introducing feedstock powders into a high temperature flame where they are rapidly molten and accelerated toward a substrate to form a coating. These coatings exhibit multi-phase microstructures, generally made up of WC, W_2C, W, and a Co-based amorphous binder (Ref 3, 4).

The WC-Co coatings work particularly well in abrasive conditions (Ref 5, 6). In the case of two surfaces in relative movement, abrasive wear results from the displacement or removal of material due to the presence of hard protuberances in one or both of these two surfaces (two-body abrasive wear) (Ref 7). Abrasive wear can also be caused by the debris (hard particles) that is free to roll and slide between two surfaces (three-body abrasive wear). When contacting surfaces move relative to each other, the friction between the two surfaces converts kinetic energy into thermal energy, or heat. When WC-Co coatings are wear tested, the resulting heat promotes the formation of oxides, mainly CoO and WO_3, with the latter having good lubricant properties (Ref 8, 9). Ball-on-disk tribometers are extensively used in determining coating friction and wear characteristics.

Solid particle erosion is a serious problem for industrial equipment, such as the walls of pipelines used for the pneumatic transportation of pulverized coal in power stations. The gas-blast method of erosion testing is widely used to evaluate the erosion resistance of many materials. In this method, abrasive particles are accelerated in a gas stream along a nozzle before they strike the specimen. Erosion can occur in two different regimes: ductile, or brittle. The erosion rate depends on the abrasive particle impact angle. In a ductile regime, the erosion rate peaks at angles lower than 90°, whereas in a brittle regime, the erosion rate peaks at 90° (Ref 10, 11). Studies by Anand and Conrad (Ref 12) in sintered WC-Co materials established that the erosion behavior of WC-Co alloys could be changed from a brittle type, characterized by maximum erosion at 90°, to a ductile type with maximum erosion at lower angles, by decreasing WC grain size or by increasing erodent particle size and velocity. In WC-Co coatings, however, erosion behavior is not much clear, and the effect of microstructure on erosion resistance is not clearly understood.

This study was undertaken to examine the wear and erosion behavior of WC-Co plasma-sprayed coatings obtained from micrometric (conventional) and nanometric feedstocks. In a previous study (Ref 13), the influence of

V. Bonache, M.D. Salvador, and **J.C. García**, Instituto de Tecnología de Materiales, Universidad Politécnica de Valencia, Valencia, Spain; and **E. Sánchez** and **E. Bannier**, Instituto de Tecnología Cerámica, Asociación de Investigación de las Industrias Cerámicas, Universitat Jaume I, Castellón, Spain. Contact e-mail: enrique.sanchez@itc.uji.es.

plasmogenous gases on mechanical properties and wear behavior was studied. This article is focused on the study of the effect of plasma intensity on wear and erosion resistance. The study particularly analyzed wear and erosion mechanisms and the variation of the friction coefficient with sliding distance.

2. Experimental Procedure

2.1 Materials

Two types of WC-Co powders were used: micrometric powder and nanometric powder. Powder composition, agglomerate, and particle size are detailed in Table 1. The test powder morphologies are shown in Fig. 1.

2.2 Coating Processing

The coatings were obtained by atmospheric plasma spraying (APS) using a Sulzer-Metco F4 MB plasma gun, operated by an industrial robot. Before spraying, the substrate was grit-blasted with corundum at a pressure of 3.2 bar and cleaned using ethanol to remove remaining dust or grease from the surface. During the process, the material to be deposited was injected in powder form using argon as carrier gas. The main spraying parameters are given in Table 2.

Three plasma intensities (475, 625, and 725 A) and alternate micrometric and nanometric feedstocks were used to obtain six coatings, as shown in Table 3. The powder feed and gas flow rate were maintained constant during the spraying of all the coatings.

Table 1 Characteristics of the powders used

Powder	Supplier	Reference	Composition	Agglomerate size, μm	Particle size, nm
Conventional	Sulzer-Metco	METCO 72F-NS	WC-12 wt.%Co	15-45	500-2000
Nanometric	Inframat AM	Infralloy S7412	WC-12 wt.%Co	5-45	50-500

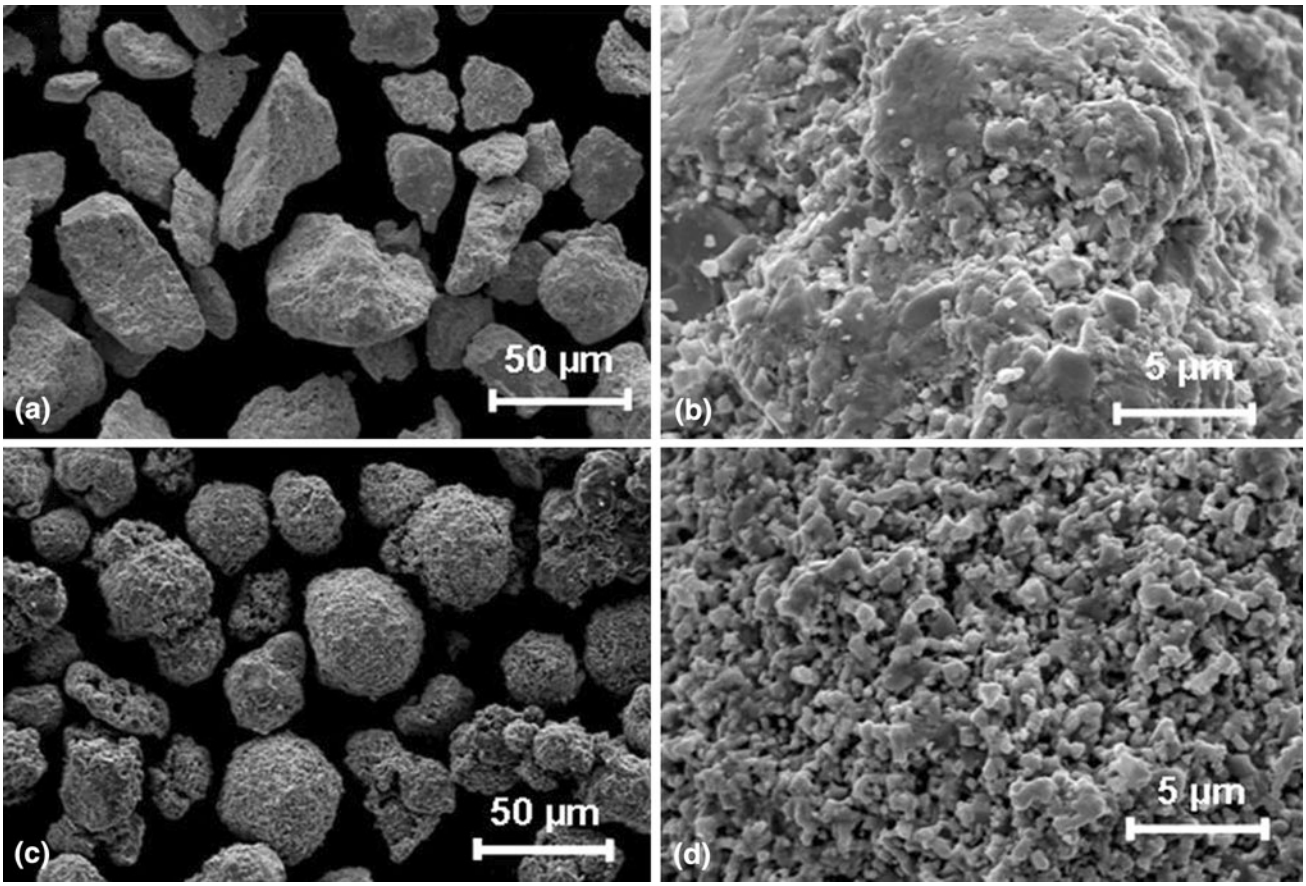

Fig. 1 FESEM micrographs (secondary electron images, SEI) of the two powders used in the study: (a) micrometric (low magnification), (b) micrometric (high magnification), (c) nanometric (low magnification), and (d) nanometric (high magnification)

Table 2 Spraying parameters

Parameter	Ar, slpm	He, slpm	Plasma arc intensity, A	Spraying distance, mm	Spraying velocity, m/s	Mass rate, g/min
Standard conditions	60	120	625	110	1	30
Variation	…	…	475-725	…	…	…

slpm: standard litre per minute

Table 3 Coatings deposited with different plasma intensities, alternately using micrometric and nanometric powders

Plasma intensity used, A	Powder	Coating reference
475	Micrometric	m-475
475	Nanometric	n-475
625	Micrometric	m-625
625	Nanometric	n-625
725	Micrometric	m-725
725	Nanometric	n-725

2.3 Coating Characterization

X-ray diffraction (XRD) with Cu Kα radiation was used to identify the phases present in the coatings. A scanning electron microscope coupled with an energy-dispersive x-ray spectrometer (EDX) was used to study the powders and the as-sprayed coatings, and to analyze the abraded surfaces. Porosity was measured by image analysis, performed by thresholding cross-sectional images and given an area fraction. All the porosity values mentioned represents the percentage of cross-sectional area occupied by pores. Microhardness tests were conducted with a 500-g load and dwell time of 15 s, using a Matsuzawa MHT2 microhardness tester. Fracture toughness (K_{IC}) was estimated by the Vickers indentation technique at 1-kg load. The Lawn and Fuller equation was used to calculate toughness (Ref 14).

$$K_{IC} = 0.0515\frac{P}{c^{3/2}} \quad \text{(Eq 1)}$$

The wear and erosion tests have been carried out on the as-sprayed coatings, without surface preparation. The surface properties of as-sprayed coatings and wear tracks were evaluated using the Mahr Perthometer equipped with MarSurf XR 20 software. The roughness values (R_a and R_z) were obtained by averaging four sets of data.

The friction and wear tests were conducted using a ball-on-disk arrangement on a Microtest MT2/60/SCM/T Tribometer operating under dry conditions. Si_3N_4 balls ($HV_{0.5\ kg} = 1760 \pm 21$), 4 mm in diameter, were used in the tests. Four sliding distances (70, 500, 1000, and 2000 m), with a load of 50 N at a sliding speed of 0.1 m/s were used in the wear and friction tests. Before and after a wear test, the specimens were cleaned by means of compressed air and brushing, and were kept in ultrasounds for 15 min. Mass loss was determined by weighing the samples before and after the test using a microbalance with an accuracy of ±0.1 mg. The wear rate (wr) was determined from the following equation:

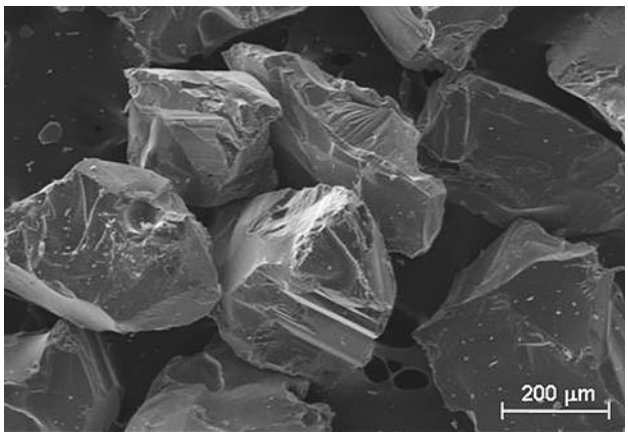

Fig. 2 FESEM micrograph of the erodent (Al_2O_3) used in the erosion tests

$$\text{wr} = \frac{m}{L \cdot D} \quad \text{(Eq 2)}$$

where m (kg) is sample mass loss, L (N) is applied load, and D (m) is sliding distance.

Erosion tests were performed with a gas blasting apparatus. The nozzle has an internal diameter of 3 mm, and the specimen is placed at a distance of 15 mm from the nozzle. Two impact angles were used in the tests (45° and 90°). The cleaning procedure was the same as that described above for the wear tests. Mass loss was also determined by weighing the samples before and after the test, using an electronic precision balance with an accuracy of ±0.1 mg. The erosion rate (ε) was determined from the following equation:

$$\varepsilon = \frac{m}{M} \quad \text{(Eq 3)}$$

where m (g) is the mass lost by the sample during the erosion test, and M (g) is the erodent mass that impacts the sample. Al_2O_3 of size 250 µm (see Fig. 2) was used as an erodent in all tests.

3. Results and Discussion

3.1 Microstructural Characterization

SEM and XRD analysis of the coatings showed that they consisted of WC grains, and two secondary phases

(W_2C and W) embedded in a Co-rich matrix. WC was present in the initial powder, but the secondary phases formed during the spraying process through WC particle decarburization (Ref 15). XRD analysis (Fig. 3) also revealed that the W_2C and W contents increased when plasma intensity was raised (the W_2C and W peaks are higher). This is logical, because the decarburization process is encouraged when plasma energy is increased. Coating thickness was about 200 μm, as may be observed in Fig. 4(a). Figure 4(b) shows that the coatings exhibit the typical microstructure of thermal sprayed WC-12Co coatings, containing WC grains and large areas of Co with a high quantity of dissolved W.

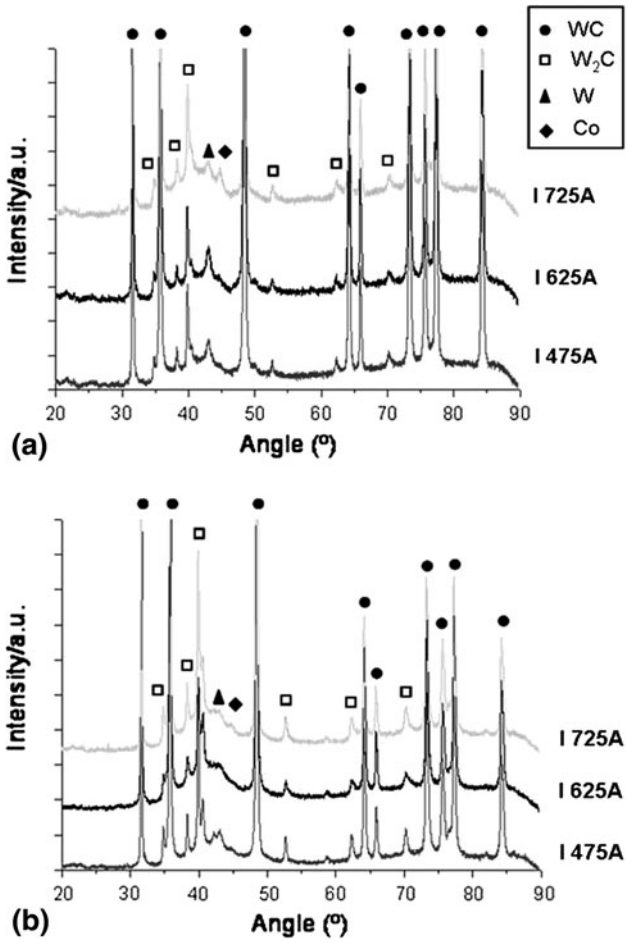

Fig. 3 XRD diffraction patterns of coatings sprayed using (a) conventional powder and (b) nanometric powder

The presence of molten and unmolten areas largely depends on plasma intensity, as may be observed in Fig. 5. At higher plasma intensity, the fully molten regions increase. This has a great influence on coating wear and erosion behavior. Coating porosity is plotted against plasma intensity in Fig. 6(a). For micrometric coatings, porosity changes drastically with plasma intensity and minimizes at a plasma intensity of 625 A. At low intensity (475 A), plasma energy is not high enough to melt micrometric powder. This is the main reason for the high porosity values attained at this intensity. However, at 625 and 725 A, the plasma energy allows micrometric powder to be almost completely molten. On the other hand, in nanometric coatings, porosity is not significantly affected by plasma intensity. In fact, the porosity found in these coatings is associated to that found originally in the feedstock. This kind of porosity is constituted by smaller pores that are present in the initial powder and is difficult to remove during plasma spraying. Zhao et al. (Ref 16) have also reported that nanometric WC-12Co coatings deposited by APS present smaller pores than micrometric ones.

3.2 Mechanical Properties

Vickers microhardness and toughness are plotted against plasma intensity for each coating in Fig. 6(b). The highest microhardness and toughness values are obtained at a plasma intensity of 625 A for both micrometric and nanometric coatings. However, the effect of feedstock

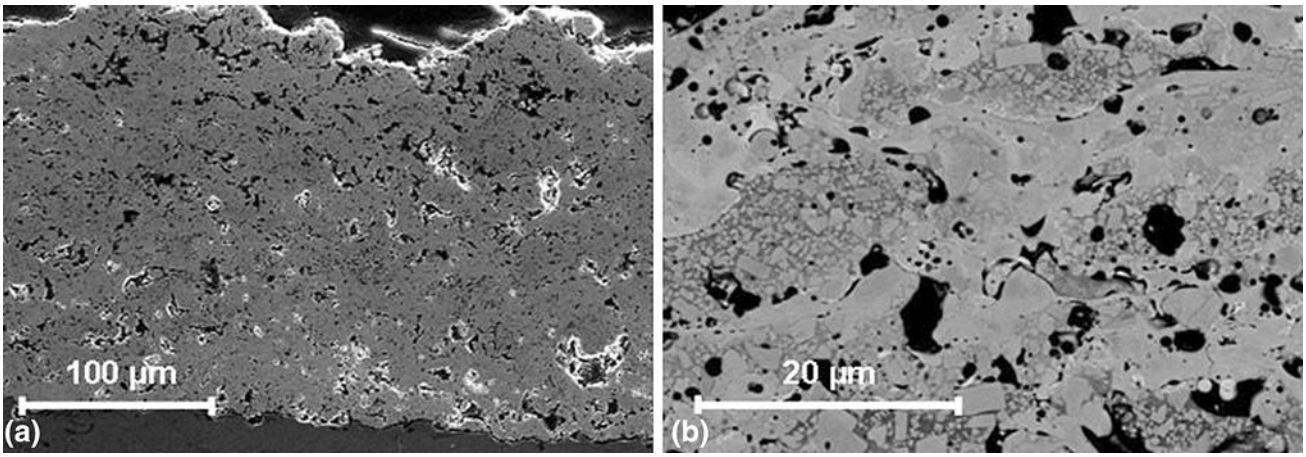

Fig. 4 Cross-sectional SEM images of nanometric coating sprayed using an intensity of 625 A: (a) low magnification SE micrograph and (b) high magnification BSE micrograph

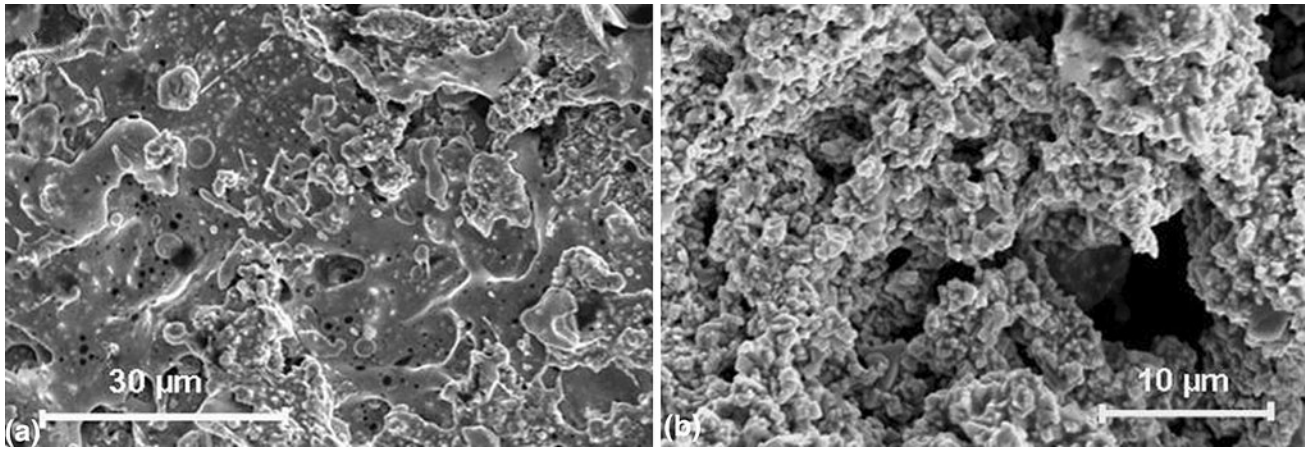

Fig. 5 SE-SEM images of a plan view of the as-sprayed coatings: (a) m-725 and (b) m-475

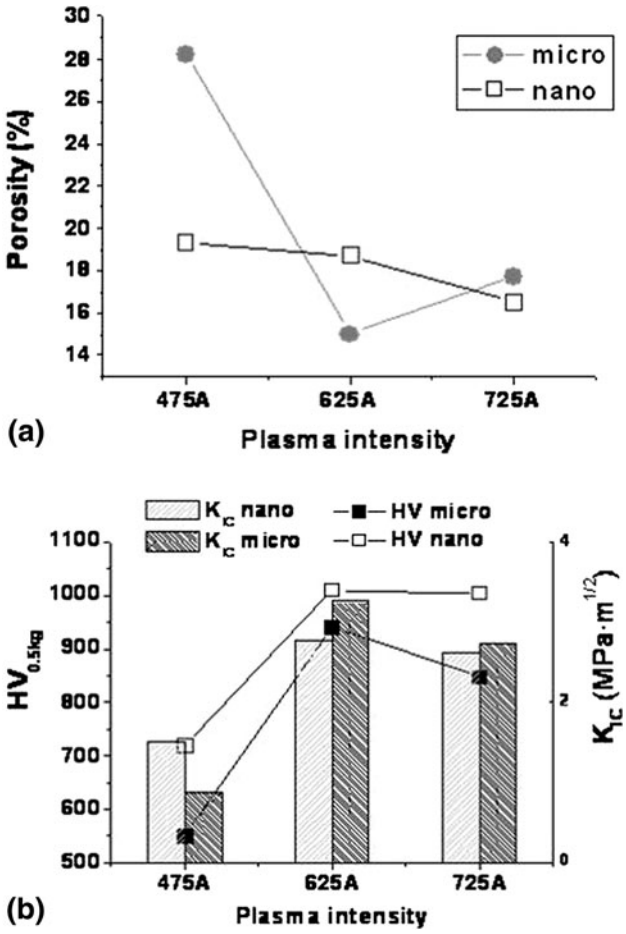

Fig. 6 (a) Porosity and (b) Vickers microhardness and toughness obtained for the coatings tested

powder particle size on microhardness and toughness is not as clear.

The increase in mechanical properties (microhardness and toughness) for micrometric coatings when plasma intensity is changed from 475 to 625 A is associated with the decrease in porosity. The lower values found at 725 A are related to a slight porosity increase associated to some gas formation together with WC decomposition and dissolution. An increase in microhardness is to be expected when the WC grain content in the coating microstructure is larger. In addition, the highest toughness values were obtained with a plasma intensity of 625 A. At 725 A, the Co matrix contained more regions in which the WC grains had completely dissolved. These regions are more brittle and cracks can therefore propagate more readily.

In the case of nanometric coatings, as the variation in macroporosity is not important, the differences observed at the lower power input is associated to a lack of cohesion in the splats and the small porosity not quantifiable by the image analysis performed.

Table 4 Surface properties of as-sprayed coatings

Sample	m-475	m-625	m-725	n-475	n-625	n-725
R_a, µm	9.0	7.9	7.8	7.6	7.9	7.3
R_z, µm	51.7	40.6	42.9	43.5	44.2	41.8

3.3 Wear and Tribological Behavior

Since surface roughness has a great effect on coating wear and erosion behavior (Ref 17), the surface properties of the as-sprayed coatings needed to be determined. Table 4 details some surface properties of interest.

The wear rates of all the tested coatings are plotted in Fig. 7. The effect of plasma intensity is observed to be more important for the coatings sprayed with micrometric powder. The minimum wear rate for micrometric coatings is reached at an intensity of 625 A. For nanometric coatings, the wear rate does not change appreciably from 475 to 625 A, though it begins to increase at 725 A. The meaningful decrease in wear rate for micrometric coatings when plasma intensity is changed from 475 to 625 A is associated with an important decrease in porosity. The general tendency observed in micrometric coatings is that wear rate decreases as mechanical properties (microhardness and toughness) increase, as expected. However, in

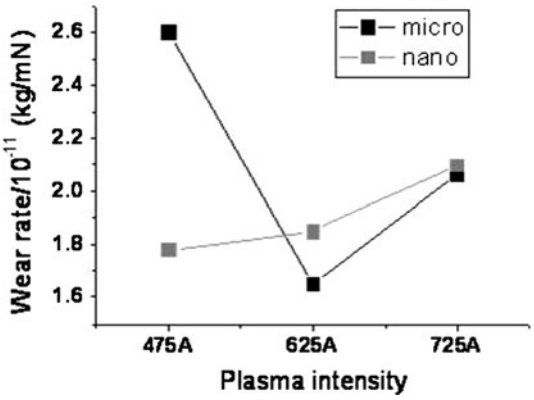

Fig. 7 Sliding wear rates and as a function of plasma intensity for micrometric and nanometric coatings

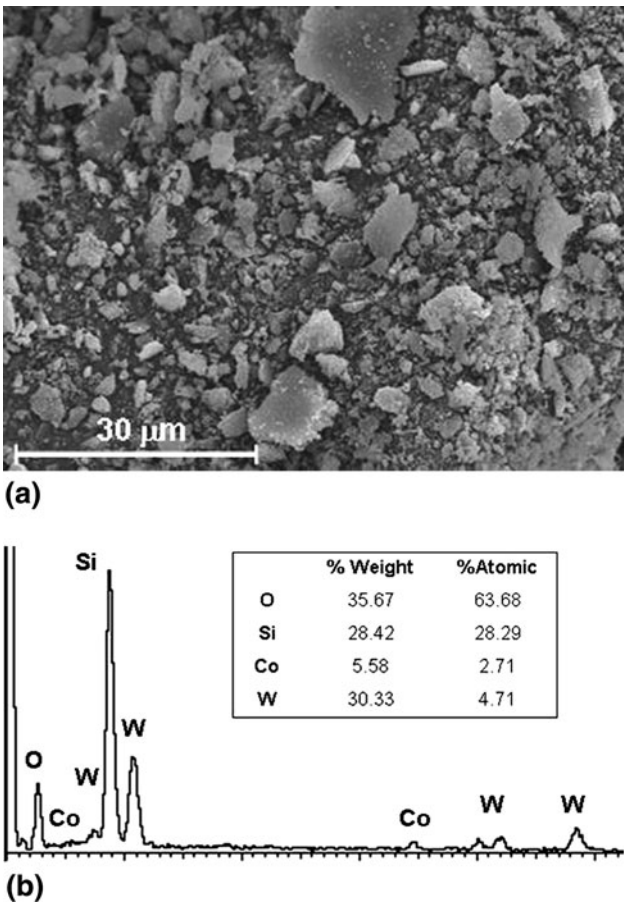

Fig. 8 (a) Wear debris generated in the pin-on-disk test of the m-625 sample and (b) EDX analysis of the wear debris

the case of nanometric coatings, a correlation between hardness and wear rate has not been found.

Debris was generated during the pin-on-disk tests, suggesting thereby that wear occurred by a three-body abrasive mechanism in all coatings. Debris was found to have a significant effect on the friction coefficient and wear processes that occurred at rolling and sliding contacts. Wear debris particle size ranged from 200 nm to

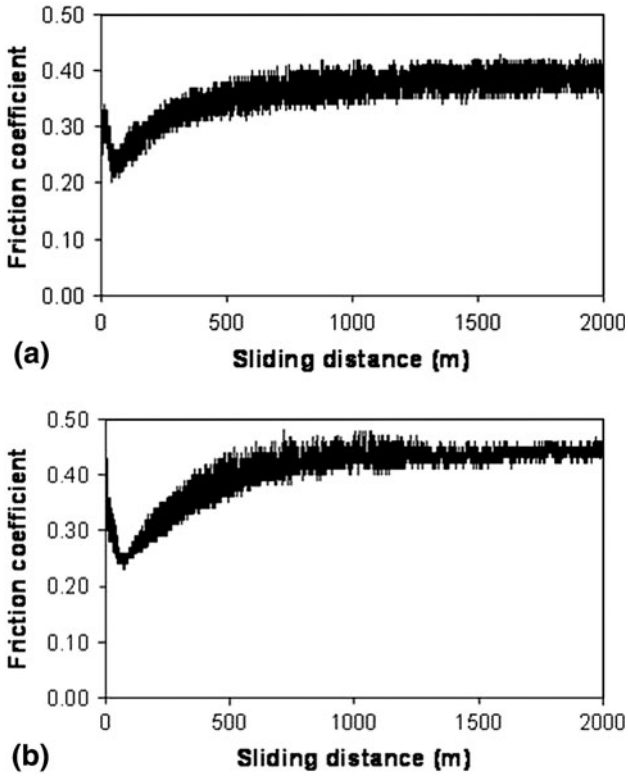

Fig. 9 Variation of the friction coefficient with sliding distance for (a) m-625 coating and (b) n-625 coating

20 μm. Debris morphology is shown in Fig. 8(a). It has been reported (Ref 18) that in humid environments (relative humidity >45%), Si_3N_4 forms silica, leading to hydrated silica film formation at the interface between the ball and the sample. Since the film is soft and has low shear strength, it reduces the friction coefficient. However, the film can be readily removed at high loads. The relative humidity measured during the test was 65%, so that silica film should have formed. In addition, the load acting on the film was very high, because the contact area was very small. This presumably resulted in film fragmentation and, hence, formation of SiO_2 debris. Figure 8(b) shows that the debris consisted mainly of Si and O (approximately in the atomic proportion of SiO_2), thus confirming the formation and fragmentation of the silica film.

Figure 9 shows the variation of the friction coefficient with distance for m-625 and n-625 coatings. For the sake of simplicity, plots are only presented of the values for these two coatings, though the tendency was similar for all studied coatings.

Figure 9 shows that the friction coefficient is not constant with distance. This could be because of the variation in the load acting on the sample because of ball wear. However, this variation in the friction coefficient might be caused by other reasons. The friction coefficient minimizes at a distance of about 70 m, after which it increases with distance. In the model developed by Zhang et al. (Ref 19), when two surfaces are in contact, part of the load, P_a, is carried by asperity contact over an area, A_a, and part of

the load, P_d, is carried by debris particles over a contact area, A_d. The friction coefficient can be described by expression 4:

$$\mu = (1 - \beta)\mu_a + \beta\mu_{ap} + \mu_d \quad \text{(Eq 4)}$$

where β is the percentage of asperity contact area in which the frictional shear stress results from ploughing, μ_a is the friction coefficient due to adhesion, μ_{ap} is the friction coefficient due to asperity ploughing, and μ_d is the friction coefficient due to debris ploughing. In order to study the variation in the friction coefficient, 70, 500, and 1000 m sliding tests were performed on the m-625 coating. The surface properties were measured and wear debris was analyzed after each test. Table 5 shows the variation of surface properties with distance.

The wear rate decreased significantly when the sliding distance was increased from 70 to 500 m, but it remained approximately constant at high sliding distances (Fig. 10). The same occurred for surface properties (Table 4), since they changed drastically at low sliding distances but stabilized when the distance increased above 70 m. In the first stage, material loss is mainly due to sample wear, but when the distance increases wear becomes more significant in the Si_3N_4 ball. This tendency was displayed in the EDX analysis of the wear debris generated at each sliding distance below. A minimum value at 70 m has been observed in the friction coefficient that is associated to the surface roughness decrease in the first stage. It can be deduced from Eq 4 that $\beta\mu_{ap}$ decreases significantly in the first phase owing to a great drop in surface roughness. At this point, the term μ_d has not changed substantially since there is not much debris yet. This could explain the minimum in the friction coefficient (μ), because at low distances the decrease in surface roughness is greater than the increase in the quantity of wear debris. When the sliding distance rises above the minimum, however, the quantity of wear debris increases (higher values of μ_d) while surface roughness does not change appreciably (the term $\beta\mu_{ap}$ is not modified). At high sliding distances, the friction coefficient is almost stable because the quantity of debris between the ball and the sample is also constant. The friction coefficient could also change with distance because of oxides formation. It is reported (Ref 20) that the high asperity flash temperatures reached during the sliding process cause coating oxidation, resulting in oxide compounds of Co and/or W. The oxide layers are easily removed by the debris generated during the test, owing to the high load acting on sample asperities. The presence of oxygen was also detected in wear track by EDX, indicating the embedding of part of these oxides in the coating.

The coating friction coefficients obtained for the last 1200 m of the sliding test are shown in Fig. 11. Note that the debris plays an important role in these friction coefficients. The friction coefficients are observed to be lower in the nanometric coatings, and the effect of intensity is more important in the micrometric coatings. In the micrometric coatings, the friction coefficient tends to increase with plasma intensity, whereas in the nanometric coatings, there is no definite tendency.

Several wear mechanisms were found in this study, but it was demonstrated by SEM that the removal of large areas of coating by sub-surface cracking was the most important mechanism. Kim et al. (Ref 21) have also argued that extension of sub-surface transverse cracks is the controlling factor for material removal in abrasive wear of plasma sprayed WC-Co coatings. The formation of sub-surface transverse cracks in the coating has been observed in SEM cross-sectional micrographs according to study by Zhu et al. (Ref 22) that found the same wear mechanism in plasma sprayed coatings. SEM analysis of the wear debris confirmed, further, that large areas of coating were removed. Figure 12(a) and (b) shows BSE-SEM images of the debris generated during the wear tests. EDX showed (Fig. 12c) that the light-colored particles,

Table 5 Surface properties of the m-625 coating at different sliding distances

Sliding distance, m	70	500	1000	2000
R_a, μm	3.0	2.9	2.8	2.8
R_z, μm	17.2	14.1	13.2	13.5

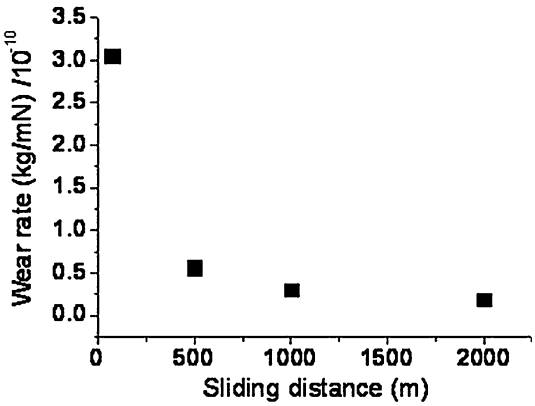

Fig. 10 Variation of wear rate with sliding distance. Sample: m-625 coating. Ball: Si_3N_4

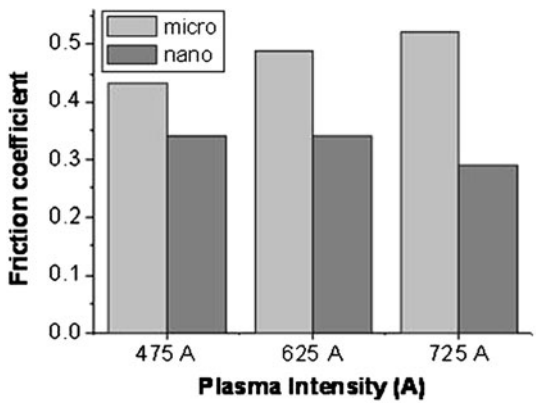

Fig. 11 Mean friction coefficient values for the last 1200 m of the sliding test

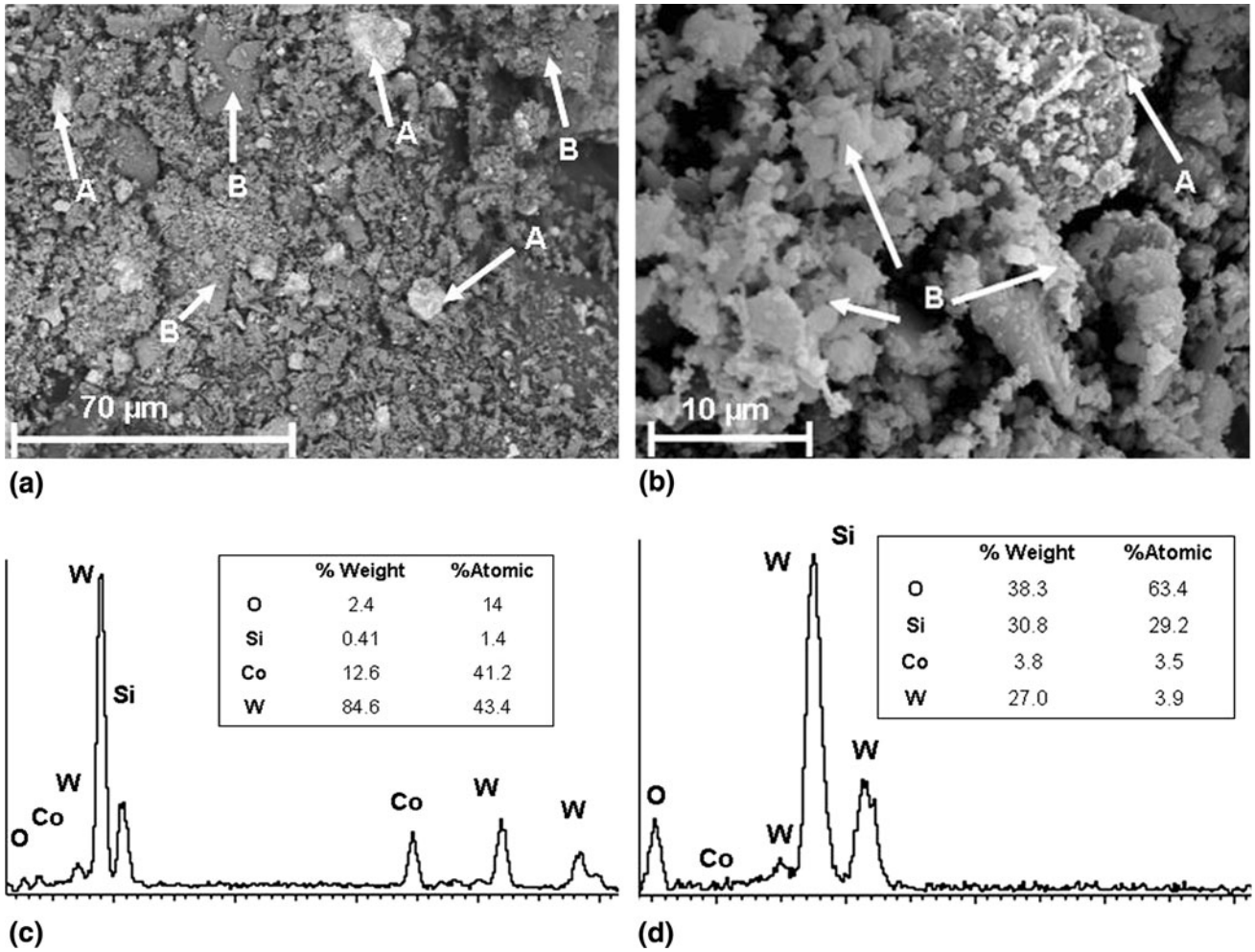

Fig. 12 Debris generated in the sliding test of the n-625 coating: low magnification BSE-SEM micrograph (a), high magnification SE-SEM micrograph (b). EDX analysis of A particles (c) and B particles (d)

marked by the letter A, correspond to WC-12Co coating fragments that were removed during the wear test. The remaining particles (gray particles), marked by the letter B, consist mainly of Si and O (Fig. 12d), suggesting that SiO_2 particles are involved. Figure 12(b) shows a high magnification SE-SEM micrograph of a coating fragment in which the size is observed to be above 15 μm, confirming the removal of large areas of coating.

The increase in wear rate when plasma intensity is raised from 625 to 725 A is associated with the change in phase composition. As mentioned before, at 725 A, the Co matrix contained more brittle regions where WC grains had completely dissolved. Due to the brittleness of these regions, wear by formation of sub-surface transverse cracks (main wear mechanism) is promoted in coatings sprayed at 725 A.

Moreover, other wear mechanisms were also observed on the wear tracks, as observed in Fig. 13: Embedded SiO_2 debris that promotes crack formation, grooving due to the rolling of debris and ploughing associated to the micro-abrasion of pulled out WC grains.

3.4 Erosion Behavior

It must be taken into account, first, that the coatings were not ground before the erosion tests. As reported by Murthy et al. (Ref 17), grinding and polishing processes affect coating erosion resistance. Figure 14 illustrates the relationship between erosion rate and impact angle for each WC-Co coating, using Al_2O_3 erosive particles. Figure 14 shows that plasma intensity had a major effect on the micrometric coatings. At an impact angle of 90° the greatest erosion resistance is attained at a plasma intensity of 625 A for both micrometric and nanometric coatings. At 45°, however, the erosion rate tends to decrease as the plasma intensity increases for micrometric coatings, though the erosion rate also minimizes at a plasma intensity of 625 A in the nanometric coatings.

Studies have demonstrated that, in brittle materials, the maximum erosion rate occurs at 90° and decreases as the angle of impact becomes more oblique (Ref 10, 23, 24). From this assumption, it is deduced that the m-625 coating exhibits the most ductile erosion behavior while the m-725

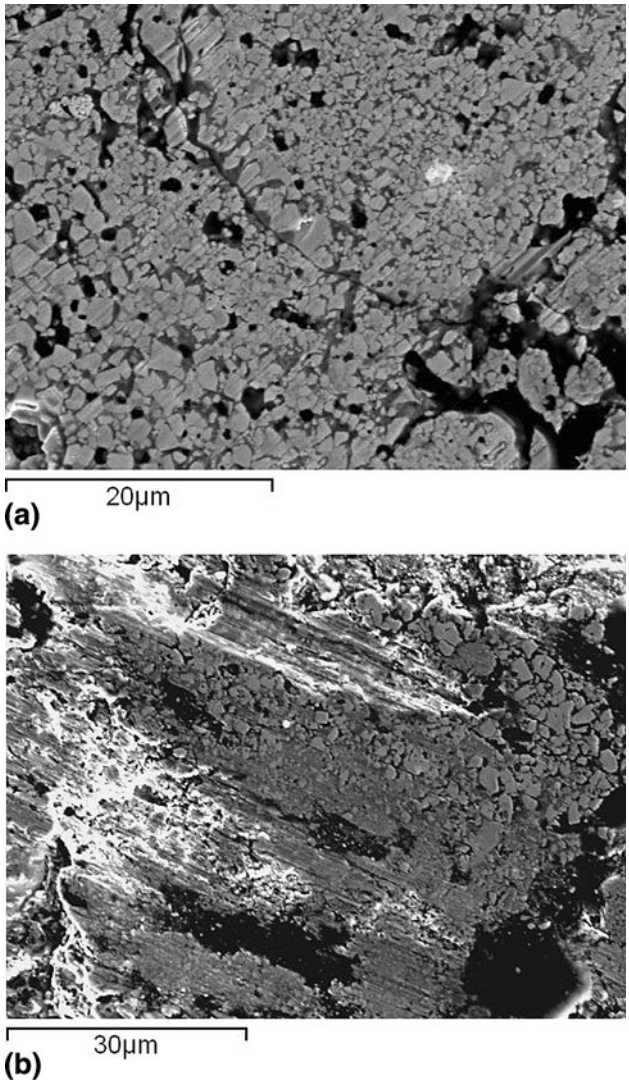

Fig. 13 Image of the wear mechanisms observed on the wear tracks

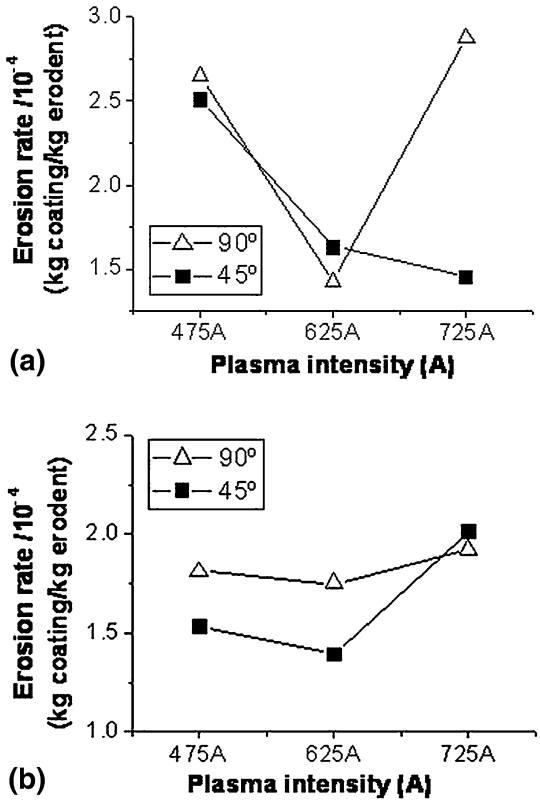

Fig. 14 Erosion rates as a function of intensity for (a) micrometric coatings, (b) nanometric coatings

coating displays the most brittle behavior. Erosion mechanisms were studied by SEM, as Fig. 15 shows. The coatings displayed little difference in the erosion mechanisms, since erosion wholly occurred mainly because of a cracking and chipping mechanism. Cracking is assumed to form first at the ''splat boundary'' during particle impact, as reported by Wang and Shui (Ref 25). Figure 15(a) shows the cross section of an eroded coating in which this erosion mechanism can be observed. It can be seen that radial and lateral cracks have been generated (under continual impacting of particles), and fractured pieces have been chipped off. Some differences were also noted between erosion at 45° and at 90°. When the impacts occurred at an angle of 45°, deeper grooves formed along the particle impact direction as a result of ploughing of erodent particles in the coating (Fig. 15b). Figure 15(c) and (d) show the damage produced by a single particle impacting at an angle of 45° and 90°, respectively. The impact direction at 45° is marked by a white arrow. The damage produced at both angles is quite different, and it can be seen that the ploughing mechanism is not as significant at 90° as at 45°.

4. Conclusions

This study has examined the effect of plasma intensity on the microstructure and tribological properties of WC-Co APS coatings obtained from conventional and nanostructured feedstocks. The findings show that plasma intensity has a great effect on porosity, phase composition, and the presence of unmolten areas. The study also shows that plasma intensity did affect the wear and erosion behavior of micrometric coatings more than it did those of nanometric coatings and that, in general, the greatest wear and erosion resistance was achieved with a plasma intensity of 625 A.

It was further found that wear occurred by a three-body abrasive mechanism and that the wear debris consisted mainly of SiO_2 fragments from Si_3N_4 ball oxidation. Surface roughness and wear rate changed drastically at the beginning of the ball-on-disk tests, but they remained approximately constant after the first 70 m, suggesting that wear debris has a marked influence on the friction coefficient and wear processes that occur at rolling and sliding contacts. In all coatings, wear was dominated by coating spallation produced by sub-surface cracking,

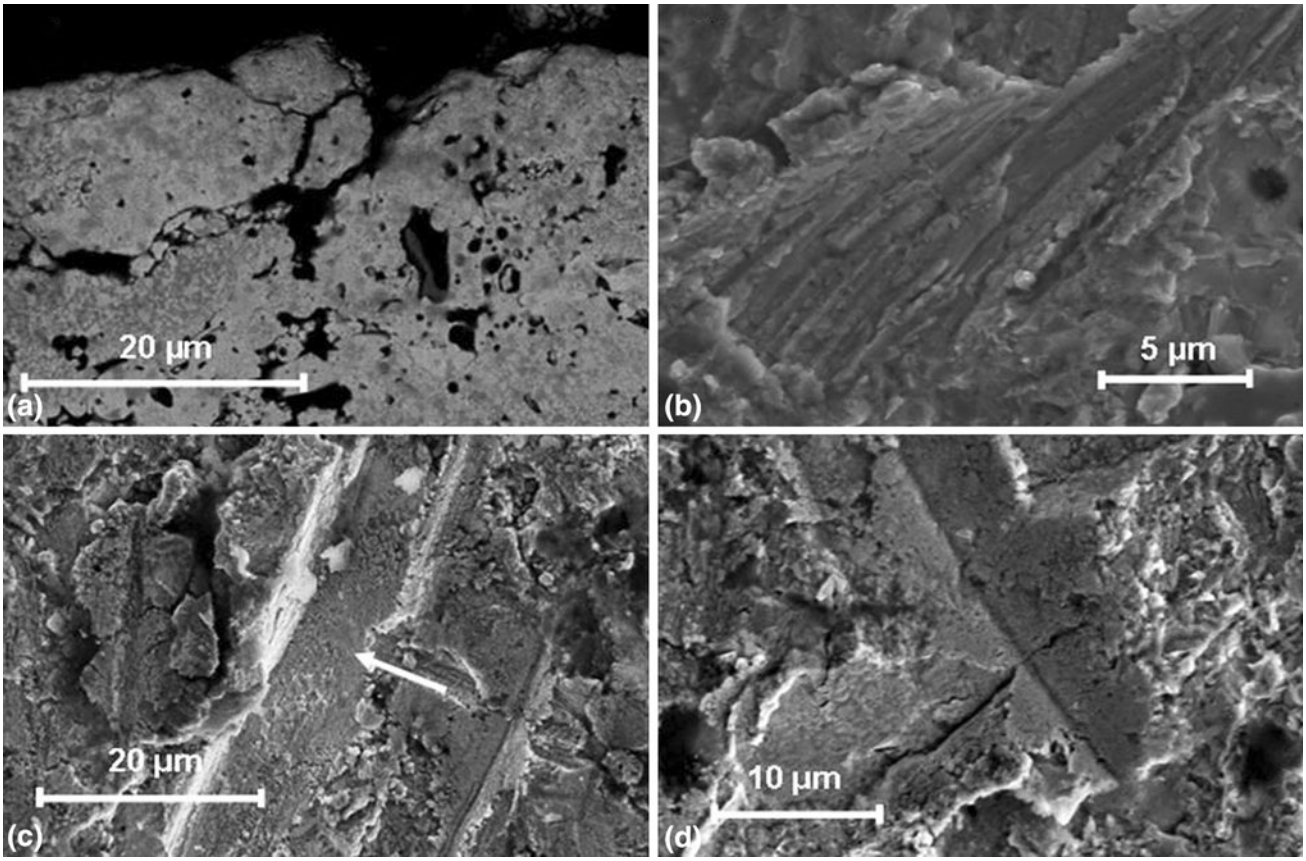

Fig. 15 Erosion wear mechanisms in: cross section of the n-725 coating at 90° (a); plan view of the n-625 coating at 45° (b); plan view of the m-475 coating at 45° (c); and plan view of the m-475 coating at 90° (d)

though other secondary wear mechanisms were also observed.

Erosion occurred mainly by a cracking and chipping mechanism from continual particle impacting, in all the studied coatings. In general, the erosion rate was greatest at 90°, indicating a brittle erosion mechanism.

Acknowledgments

This study has been conducted with the support of the Spanish Ministry of Education and Science under projects MAT 2006-12945 and MAT 2009-14144.

References

1. C. Chuanxian, H. Bingtain, and L. Huiling, Plasma-Sprayed Wear-Resistant Ceramic and Cermet Coating Materials, *Thin Solid Films*, 1984, **118**, p 485-493
2. M. Barletta, G. Bolelli, B. Bonferroni, and L. Lusvarghi, Wear and Corrosion Behavior of HVOF-Sprayed WC-CoCr Coatings on Al Alloys, *J. Therm. Spray Technol.*, 2010, **19**(1-2), p 358-367
3. C.J. Li, A. Ohmori, and Y. Harada, Effect of Powder Structure on the Structure of Thermally Sprayed WC-Co Coatings, *J. Mater. Sci.*, 1996, **31**, p 785-794
4. C. Verdon, A. Karimi, and J.L. Martin, A Study of High Velocity Oxy-Fuel Thermally Sprayed Tungsten Carbide Based Coatings. Part 1: Microstructures, *Mater. Sci. Eng. A*, 1998, **246**, p 11-24
5. S.Y. Hwang, B.G. Seong, and M.C. Kim, Characterization of WC-Co Coatings Using HP/HVOF Process, *Thermal Spray: Practical Solutions for Engineering Problems*, C.C. Berndt, Ed., ASM, Metals Park, OH, 1996, p 107-112
6. M.S.A. Khan and T.W. Clyne, Microstructure and Abrasion Resistance of Plasma Sprayed Cermet Coating, *Thermal Spray: Practical Solutions for Engineering Problems*, C.C. Berndt, Ed., ASM, Metals Park, OH, 1996, p 113-122
7. K.-H. Zum Gahr, *Microstructure and Wear of Materials*, Elsevier, Amsterdam, 1987
8. J. Li, Y. Zhang, J. Huang, and C. Ding, Mechanical and Tribological Properties of Plasma-Sprayed Cr_3C_2-NiCr, WC-Co, and Cr_2O_3 Coatings, *J. Therm. Spray Technol.*, 1998, **7**, p 242-246
9. V. Fervel, B. Normand, H. Liao, C. Coddet, E. Bêche, and R. Berjoan, Friction and Wear Mechanisms of Thermally Sprayed Ceramic and Cermet Coatings, *Surf. Coat. Technol.*, 1999, **111**, p 255-262
10. R.G. Wellman and C. Allen, The Effects of Angle of Impact and Material Properties on the Erosion Rates of Ceramics, *Wear*, 1995, **186-187**, p 117-122
11. M. Hutchings, Transitions, Threshold Effects and Erosion Maps, *Erosion of Ceramic Materials*, J.E. Ritter, Ed., Trans Tech, Uetikon-zuerich, 1992, p 75-92
12. K. Anand and H. Conrad, Local Impact Damage and Erosion Mechanisms in WC-6 wt.%Co alloys, *Mater. Sci. Eng. A*, 1988, **105-106**, p 411-421
13. E. Sánchez, E. Bannier, M.D. Salvador, V. Bonache, J.C. García, et al., Microstructure and Wear Behavior of Conventional and Nanostructured Plasma-Sprayed WC-Co Coatings, *J. Therm. Spray Technol.*, 2010, doi:10.1007/s11666-010-9480-5
14. H.R. Lawn and E.R. Fuller, Equilibrium Penny-Like Cracks in Indentation Fracture, *J. Mater. Sci.*, 1975, **10**, p 2016-2024

15. D.A. Stewart, ''Studies on the Abrasive Wear Behaviour of HVOF WC-Co Coatings,'' Ph.D. thesis, University of Nottingham, 1998
16. X.-Q. Zhao, H.-D. Zhou, and J.-M. Che, Comparative Study of the Friction and Wear Behavior of Plasma Sprayed Conventional and Nanostructured WC-12%Co Coatings on Stainless Steel, *Mater. Sci. Eng. A*, 2006, **431**(1-2), p 290-297
17. J.K.N. Murthy, D.S. Rao, and B. Venkataraman, Effect of Grinding on the Erosion Behaviour of a WC-Co-Cr Coating Deposited by HVOF, Detonation Gun Spray Processes, *Wear*, 2001, **249**, p 592-600
18. P. Sahoo, *Engineering Tribology*, Prentice-Hall of India, New Delhi, 2005
19. J. Zhang, F.A. Moslehy, S.L. Rice, A Model for Friction in Quasi-Steady-State Sliding Part I. Derivation. *Wear*, 1991, **149**(1-2), p 1-12
20. J.M. Guilemany, J.M. Miguel, S. Vizcaino, and F. Climent, Role of Three-Body Abrasion Wear in the Sliding Wear Behaviour of WC-Co Coatings Obtained by Thermal Spraying, *Surf. Coat. Technol.*, 2001, **140**, p 141-146
21. H.J. Kim, Y.G. Kweon, and R.W. Chang, Wear and Erosion Behaviour of Plasma-Sprayed WC-Co Coatings, *J. Therm. Spray Technol.*, 1994, **3**, p 169-177
22. Y. Zhu, K. Yukimura, C. Ding, and P. Zhang, Tribological Properties of Nanostructured and Conventional WC-Co Coatings Deposited by Plasma Spraying, *Thin Solid Films*, 2001, **388**(1-2), p 277-282
23. J. Guo, B.-S. Xu, H.-D. Wang, Y. Liang, Q.-F. Li, S.-C. Wei, and X. Cui, Erosion Behavior of EEDS Cermet Coatings, *App. Surf. Sci.*, 2008, **254**(17), p 5470-5474
24. Z. Feng and A. Ball, The Erosion of Four Materials Using Seven Erodents—Towards an Understanding, *Wear*, 1999, **233-235**, p 674-684
25. B.Q. Wang and Z.R. Shui, Hot Erosion Behavior of Carbide-Metal Composite Coatings, *J. Mater. Proc. Technol.*, 2003, **143-144**, p 87-92